ARMY RESEARCH LABORATORY

Doppler Processing with Ultra-wideband (UWB) Impulse Radar

by Traian Dogaru

ARL-TN-0529 **March 2013**

NOTICES

Disclaimers

The findings in this report are not to be construed as an official Department of the Army position unless so designated by other authorized documents.

Citation of manufacturer's or trade names does not constitute an official endorsement or approval of the use thereof.

Destroy this report when it is no longer needed. Do not return it to the originator.

Army Research Laboratory
Adelphi, MD 20783-1197

ARL-TN-0529 **March 2013**

Doppler Processing with Ultra-wideband (UWB) Impulse Radar

Traian Dogaru
Sensors and Electron Devices Directorate, ARL

REPORT DOCUMENTATION PAGE

Form Approved
OMB No. 0704-0188

1. REPORT DATE *(DD-MM-YYYY)*	2. REPORT TYPE	3. DATES COVERED (From - To)
March 2013	Final	1 January 2013

4. TITLE AND SUBTITLE
Doppler Processing with Ultra-wideband (UWB) Impulse Radar

5a. CONTRACT NUMBER

5b. GRANT NUMBER

5c. PROGRAM ELEMENT NUMBER

6. AUTHOR(S)
Traian Dogaru

5d. PROJECT NUMBER

5e. TASK NUMBER

5f. WORK UNIT NUMBER

7. PERFORMING ORGANIZATION NAME(S) AND ADDRESS(ES)
U.S. Army Research Laboratory
ATTN: RDRL-SER-U
2800 Powder Mill Road
Adelphi, MD 20783-1197

8. PERFORMING ORGANIZATION REPORT NUMBER
ARL-TN-0529

9. SPONSORING/MONITORING AGENCY NAME(S) AND ADDRESS(ES)

10. SPONSOR/MONITOR'S ACRONYM(S)

11. SPONSOR/MONITOR'S REPORT NUMBER(S)

12. DISTRIBUTION/AVAILABILITY STATEMENT
Approved for public release; distribution unlimited.

13. SUPPLEMENTARY NOTES

14. ABSTRACT
This technical note analyzes the possibility of performing radar Doppler processing with ultra-wideband (UWB) impulses. This is a departure from traditional Doppler radar implementation, which typically uses narrowband pulses. The theory of Doppler processing with UWB impulses is first presented, followed by an analysis of the Doppler resolution. Some simple simulated examples are included, involving both baseband and modulated UWB impulses. The major drawback of this technique consists of the fact that the Doppler resolution degrades proportionally with the target velocity. Consequently, this type of processing could only be applied to slow-moving targets.

15. SUBJECT TERMS
UWB radar, Doppler radar

16. SECURITY CLASSIFICATION OF:			17. LIMITATION OF ABSTRACT	18. NUMBER OF PAGES	19a. NAME OF RESPONSIBLE PERSON
a. REPORT	b. ABSTRACT	c. THIS PAGE			Traian Dogaru
Unclassified	Unclassified	Unclassified	UU	28	19b. TELEPHONE NUMBER (*Include area code*) (301) 394-1482

Standard Form 298 (Rev. 8/98)
Prescribed by ANSI Std. Z39.18

Contents

List of Figures

1. Introduction

The ultra-wideband (UWB) radar technology has emerged as a promising solution to a variety of sensing scenarios that involve short ranges, low average power, good resolution, and the ability to penetrate materials. Among the successful applications are ground penetrating radar (GPR), foliage penetrating (FOPEN) radar, and sensing through the wall (STTW) radar. The Synchronous Impulse Reconstruction (SIRE) radar (*1*), designed and built at the U.S. Army Research Laboratory (ARL), is an example of this technology. In its main operational mode, it produces high-resolution images of stationary targets while the platform is in slow motion. In this study, we investigate whether this type of radar can also be used to estimate the velocity of a moving target via Doppler processing when the platform is stationary.

Traditional Doppler analysis with pulsed radar uses narrowband pulses, which are sampled and processed coherently over a certain time interval (*2*). Although the definition of narrowband versus wideband pulses is relative, for our purpose, a pulse is considered narrowband if, during the coherent processing interval (CPI), the moving target stays within the same range resolution cell.

Recently, several papers (*3*–*4*) examined the possibility of performing Doppler analysis of a moving target using UWB (or, equivalently, high range resolution) waveforms. However, these investigations do not make any mention of the Doppler domain resolution that their methods can achieve. The study presented in this technical note attempts to establish the theoretical Doppler resolution and other performance limits for UWB radar.

The technical note is organized as following: section 2 discusses aspects of Doppler processing with UWB pulses, section 3 presents a simple numerical example, and section 4 offers conclusions.

2. Doppler Processing with UWB Pulses

2.1 UWB Pulses

In this work, we focus our attention on the processing of UWB impulses. These are impulses of very short duration (of the order of nanoseconds), with spectra ranging from near-direct-current (DC) to several GHz (typically they are used in relatively low-frequency applications, up to about 3 GHz [*1*]). Although the definition of an UWB pulse may vary from author to author, the common characteristic of these pulses is a large bandwidth-to-center-frequency ratio, of the order of unity. In terms of modulation, we distinguish two different types of UWB pulses:

unmodulated or baseband pulses (generated directly in the transmission band, as in reference 1), and modulated around a carrier frequency (such as the pulses used in reference 3).

A typical family of baseband (unmodulated) UWB waveforms is that of Rayleigh pulses (*5*), which may have different orders. Figure 1 plots the 4th order Rayleigh pulse in the time domain (figure 1a) and its spectrum magnitude (figure 1b). The red line in the time-domain plot outlines the pulse envelope (*6*). The mathematical expression of this pulse in the time domain is (*5*)

$$p(t) = \mathrm{Re}\left\{\left(\frac{j}{j + \frac{2\pi f_0 t}{4}}\right)^5\right\}. \qquad (1)$$

Notice that the Rayleigh pulse spectrum $P(f)$ is asymmetric, so we cannot speak about a "center frequency." Instead, we characterize this spectrum by the frequency of its peak, f_0. Interestingly, the bandwidth is also determined by f_0 (the 6 dB bandwidth can be expressed as $B \cong 1.5 f_0$), so only one parameter completely characterizes the pulse. Other types of baseband UWB waveforms include the Gaussian pulse and its derivatives (of first or higher order). The spectra of the Gaussian-derivative pulses look similar to those of the Rayleigh pulses and likewise, they are completely characterized by one parameter (f_0).

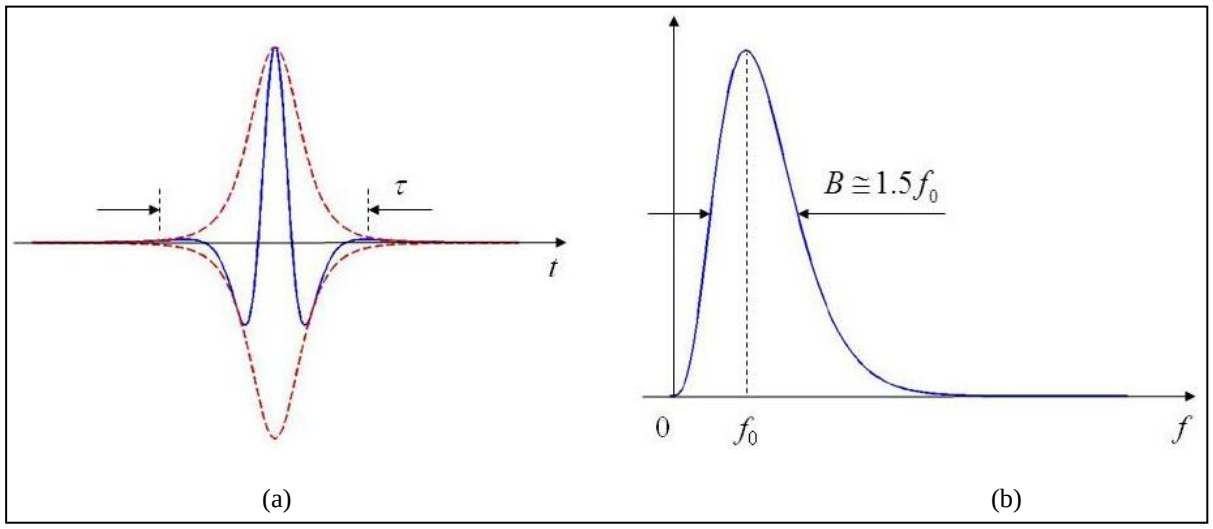

Figure 1. Representation of the 4th order Rayleigh pulse in (a) time domain and (b) frequency domain. The red curve in the time domain shows the pulse envelope.

Note: All the frequency domain magnitude plots in this report use a linear scale.

Modulated UWB pulses involve a carrier of relatively low microwave frequency, which is amplitude-modulated by an envelope with a short-pulse shape. Typically, only a few cycles of the carrier are transmitted with each pulse. A typical example is a Gaussian-modulated sinusoid, which is represented in figure 2, and can be written as

$$p(t) = e^{-(t/\tau_0)^2} \cos(2\pi f_0 t). \quad (2)$$

Notice that the spectrum of this pulse $P(f)$ is symmetric and centered at f_0 (which can now be called center frequency). The bandwidth is determined by the τ_0 parameter according to $B \cong \frac{1}{2\tau_0}$ (for the 6 dB bandwidth), while the total pulse duration is $\tau \cong 2\tau_0 \cong \frac{1}{B}$. As compared to the baseband UWB pulses, a modulated pulse is characterized by two parameters, τ_0 and f_0.

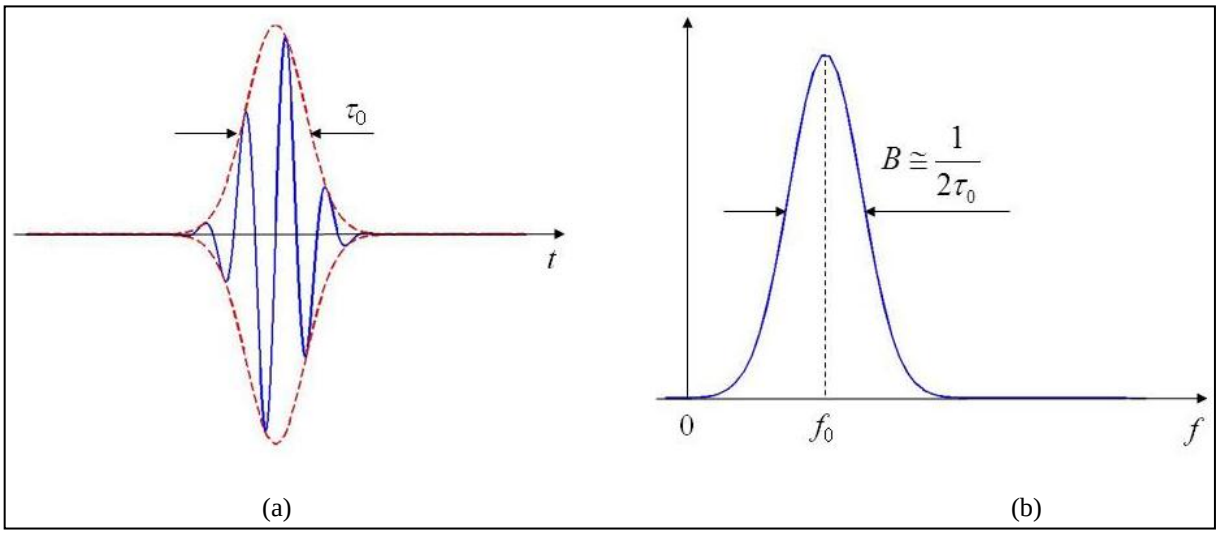

Figure 2. Representation of a Gaussian-modulated sinusoid in (a) time domain and (b) frequency domain. The red curve in the time domain shows the pulse envelope.

For reference, a narrowband pulse can be mathematically expressed as a sinusoid containing amplitude and phase modulation (*2*):

$$p(t) = A(t)\cos(2\pi f_0 t + \phi(t)). \quad (3)$$

Notice that a modulated UWB pulse can be described by the same mathematical expression as a narrowband pulse; however, we cannot reduce a baseband UWB pulse to an expression similar to equation 3. Therefore, the processing of these pulses requires a different type of mathematical treatment than conventional radar pulses.

2.2 Doppler Processing with Baseband UWB Pulses

This section shows the principle of Doppler processing that takes place in an UWB radar receiver and illustrates the processing chain with simple diagrams. The following simplifying assumptions are made: (1) there is only one point-like target, moving towards the radar at constant, positive radial velocity *v*, and placed at a range that is large enough such that the amplitude of the radar echoes does not vary from pulse to pulse; (2) the received pulse has the same shape as the transmitted pulse; and (3) no noise is present in the received signal. In addition, we make the reasonable assumption that the pulse repetition frequency (PRF) is large

enough to avoid any aliasing in the Doppler domain (*2*). In this section, we choose the 4th order Rayleigh pulse to illustrate the method; however, this applies more generally to any baseband (unmodulated) pulses that can be written as $p(t) = p(f_0 t)$ (where t and f_0 always appear together as a product).

The analog part of an UWB radar receiver is in principle very simple and includes radio-frequency (RF) filtering and amplification. No pulse compression is required in such a receiver, since the range profile is simply the envelope of the received signal. If the pulse is already in baseband, no demodulation is required either. This signal is sampled directly at a rate greater or equal to the Nyquist rate (*7*) and digitized (issues related to the limited speed of analog-to-digital converters and ways to circumvent these limitations (*1*) are not discussed here). We assume in the following that the sampling rate is close to the Nyquist rate, such that each sample corresponds to a range bin (*2*).

The Rayleigh pulse shown in figure 1 corresponds to the in-phase signal component. For Doppler processing, we need to obtain the complex envelope of this waveform (*6*), whose real part consists of the in-phase component already mentioned, while its imaginary part is the quadrature component. The latter is computed via a discrete Hilbert transform (*7*) of the in-phase component.

The following symbols will be used in this and the following section:

t –fast time (in general)

τ – pulse duration in fast time

T_r – pulse repetition interval

τ_s – pulse duration in slow time

τ_0 – pulse width parameter for modulated pulses

τ_{0d} – pulse width parameter in the Doppler domain (modulated pulses)

CPI – coherent processing interval

Δt – time shift between two pulses caused by the target motion

R – range

R_0 – target range for the first pulse in the sequence

ΔR – range displacement corresponding to Δt

f – frequency (in general)

f_0 – frequency of the pulse spectrum peak (center frequency for modulated pulses)

B – pulse bandwidth

f_{0d} – frequency of the peak in the Doppler domain

B_d – pulse bandwidth in the Doppler domain

f_r – pulse repetition frequency

v –radial velocity of the target

c – speed of light

δf – Doppler frequency resolution

δv – velocity resolution

δR – range resolution

We can rearrange the data samples in a two-dimensional (2-D) array, where each row is a range profile associated to a transmitted pulse. Thus, the row index corresponds to pulse number n (associated with its receiver turn-on time nT_r), while the column index corresponds to a sample number within a range profile. The time corresponding to range on the horizontal axis is called "fast time" (*2*), since it is measured on a scale comparable to the individual pulse duration. The time on the vertical axis is known as "slow-time," because it is measured on a scale comparable to the pulse repetition interval T_r. The 2-D data array is shown in figure 3, where the magnitude of the complex envelope is represented in dB on a pseudo-color scale.

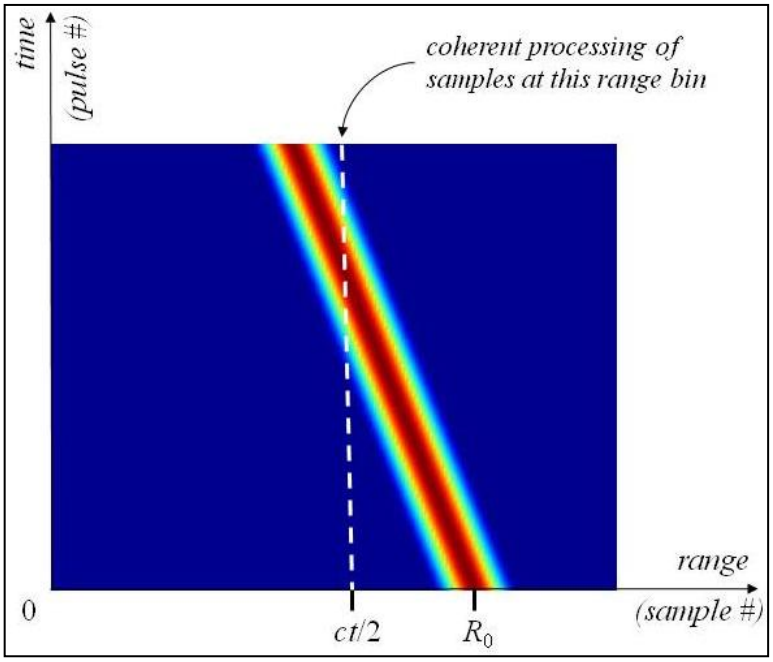

Figure 3. Representation of the 2-D received data array obtained by arranging the range profiles associated to each transmitted pulse by rows.

We compute the Doppler spectrum of the received pulses as in conventional pulsed Doppler radar by taking the discrete Fourier transform (DFT) over samples in successive range profiles corresponding to the same range bin (column-wise in the 2-D data array). The process is illustrated in figures 4 and 5. Thus, in figure 4, we show a number of overlapping received pulses on the same fast-time axis and the sampling time *t* on this axis, corresponding to the range bin $R = \frac{ct}{2}$. The pulse amplitude values at this sampling time (or range bin) are rearranged as in figure 5a, which shows the pulse samples in the slow-time domain for the in-phase component. After computing the quadrature component (figure 5b), one can obtain the samples of the complex envelope in slow time, whose DFT represents the Doppler spectrum (figure 5c). Notice that, for each pulse, the fast-time origin is the turn-on time of the receiver (the left side column of the 2-D array in figure 3), whereas the slow-time origin corresponds to the first pulse in the sequence (the bottom side row of the 2-D array in figure 3).

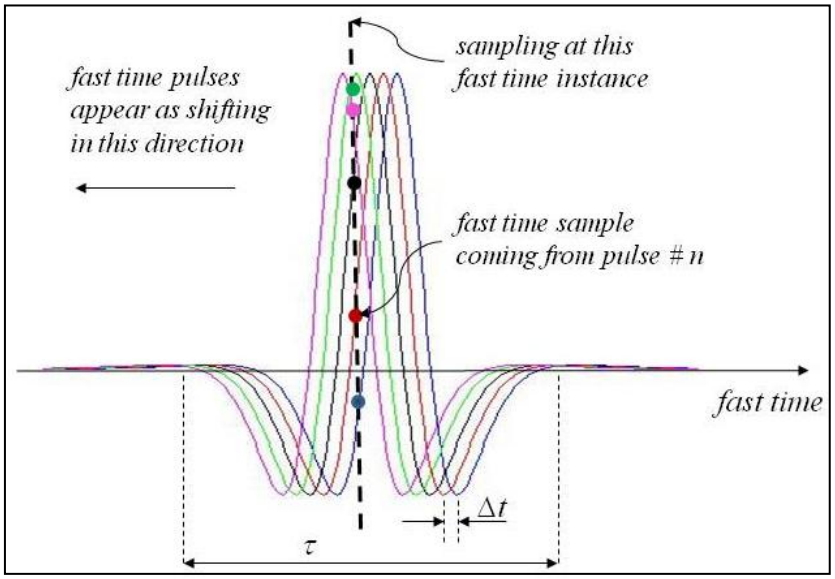

Figure 4. Sequence of overlapped received pulses in the fast-time domain illustrating the sampling procedure for Doppler processing.

Next, we need to derive an expression for the Doppler spectrum. As a reminder, the common assumptions made for narrowband pulses do not apply in the case of unmodulated baseband pulses, including the concept of a frequency deviation (Doppler shift) caused by the target motion. In reference to figure 4, the time shift between two successive pulses caused by the target motion is

$$\Delta t = \frac{2\Delta R}{c} = \frac{2T_r v}{c} = \frac{2v}{cf_r}. \tag{4}$$

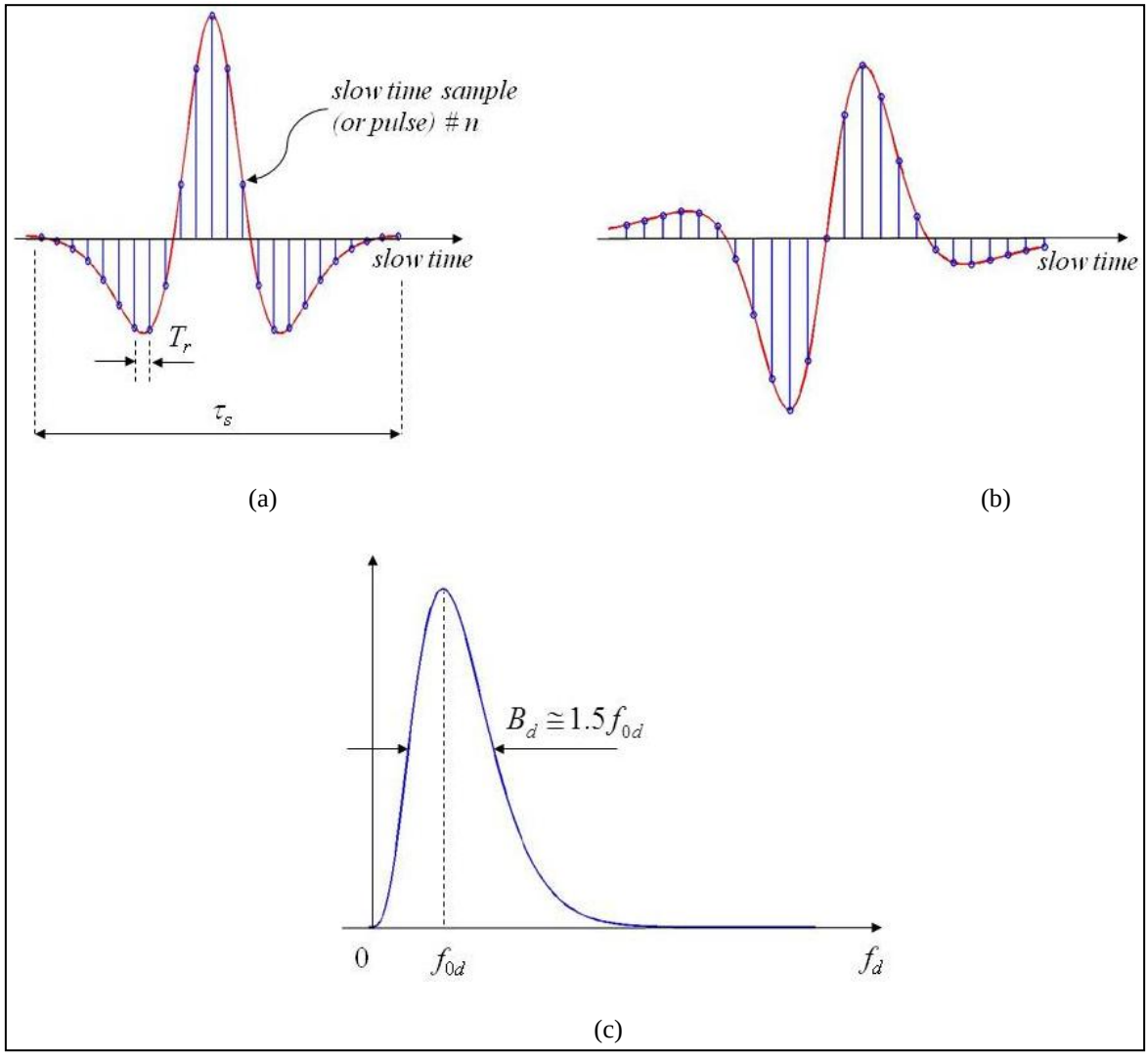

Figure 5. Representation of the sampled waveforms in the slow-time domain and their associated Doppler spectrum, showing (a) in-phase component in the slow time domain, (b) quadrature component in the slow time domain, and (c) spectrum in the Doppler frequency domain. These plots correspond to a 4th order Rayleigh pulse at transmission.

Now consider the sampled pulse $s(n)$ in the slow-time domain (figure 5a), with sampling interval T_r. By using the diagrams in figures 3 and 4, as well as equation 4, we can establish the following expressions:

$$s(n) = p\left(t - \frac{2R_0}{c} + n\Delta t\right) = p\left(t - \frac{2R_0}{c} + nT_r\frac{2v}{c}\right), \tag{5}$$

where $p(t)$ is the fast-time domain expression of the pulse (equation 1). For the sake of the argument, we compute the Doppler spectrum in figure 5c via the discrete-time Fourier transform (DTFT) (*7*). (Note: The difference between the DTFT and the DFT is that the former uses a continuous frequency variable, whereas the latter uses discrete (sampled) frequencies; extending

the proof to the sampled frequency case is straightforward). Thus, the DTFT of the signal in equation 5 is

$$S(f) = \sum_n p\left(t - \frac{2R_0}{c} + nT_r \frac{2v}{c} \right) e^{-j2\pi n T_r f} \ . \tag{6}$$

The sum over n can be extended from - ∞ to ∞, since the pulse amplitude is null outside the data window. Now consider the change of variable $m = \text{round}\left(\frac{ct - 2R_0}{2vT_r} \right) + n$:

$$S(f) = \sum_m p\left(\frac{2v}{c} m T_r \right) e^{-j2\pi m T_r f} e^{j2\pi \frac{ct - 2R_0}{2v} f} \ . \tag{7}$$

Since we are interested in the magnitude of $S(f)$, the last exponential factor does not influence the result. Moreover, the expression $\sum_m p\left(\frac{2v}{c} m T_r \right) e^{-j2\pi m T_r f}$ can be recognized as the DTFT of the pulse $p\left(\frac{2v}{c} t \right)$. Using the well-known scaling property of the Fourier transform (*6*), we can write

$$|S(f)| = \frac{c}{2v} \left| P\left(f \frac{c}{2v} \right) \right| . \tag{8}$$

This equation shows that the magnitude of the Doppler spectrum is a replica of the transmitted pulse spectrum $P(f)$, with the frequency axis scaled down by a factor $\frac{c}{2v}$. Consequently, the Doppler spectrum will have a peak corresponding to

$$f_{0d} = f_0 \frac{2v}{c} \ . \tag{9}$$

The target velocity is estimated by finding the frequency of the Doppler spectrum peak f_{0d} and using the equation

$$v = \frac{c}{2} \frac{f_{0d}}{f_0} \ . \tag{10}$$

Notice that this expression is very similar to the estimation of the target velocity in conventional narrowband Doppler radar (*2*), with the difference that f_0 does not represent the carrier (or center) frequency, but the peak of the transmitted pulse spectrum.

In practice, the target velocity is estimated at the same time as the range by creating a range-Doppler map. This is obtained from the original 2-D data array (figure 3) by taking column-wise

DFTs. The location of the magnitude peaks in the range-Doppler maps indicate the ranges and velocities of the (possibly multiple) targets in the scene.

One would also need to consider the fact that each DFT is performed over a limited slow-time interval (CPI). Therefore, a range-Doppler map gives indications about the target range and velocity only for that specific window of time. The target trajectory and velocity changes over time can be tracked by creating a succession of range-Doppler maps for different slow-time windows (instead of DFT we now talk about discrete short time Fourier transforms [STFT]). When we put together all the range-Doppler maps obtained at regular slow-time intervals we obtain the so-called joint range-time-frequency representation (JRTFR) data cube (*3*), which indicates the target response as a function of range, slow time, and Doppler frequency (velocity).

2.3 Doppler Processing with Modulated UWB Pulses

The Doppler processing chain in the case of modulated UWB pulses largely follows the same steps as for baseband pulses. The main difference is that now the model described by equation 3 is valid, so we can talk about a Doppler frequency shift (call that f_{0d}). The processing in this case involves an extra step: demodulation, which consists of multiplying the received signal by $e^{-j2\pi f_0 t}$ (in practical implementation, the complex envelope of the received signal is obtained by employing a quadrature demodulator [*2*]).

If we consider a Gaussian-modulated pulse as described in section 2.1, the sampled, slow-time representation of the complex envelope (after demodulation) is

$$s(n) = e^{-\left(\left(t-\frac{2R_0}{c}+nT_r\frac{2v}{c}\right)/\tau_0\right)^2} e^{j2\pi f_0\left(nT_r\frac{2v}{c}-\frac{2R_0}{c}\right)} . \tag{11}$$

This waveform is shown in figure 6a. Notice that, in this case, we can only represent the magnitude of the complex envelope, although a significant part of the Doppler information is contained in the phase. To underline this aspect, we preserved the sign of the phase in the slow-time domain representation (figure 6a). Figure 6b displays the corresponding Doppler spectrum, which is given by the DTFT of $s(n)$:

$$S(f) = \sum_n e^{-\left(\left(t-\frac{2R_0}{c}+nT_r\frac{2v}{c}\right)/\tau_0\right)^2} e^{j2\pi f_0\left(nT_r\frac{2v}{c}-\frac{2R_0}{c}\right)} e^{-j2\pi nT_r f} . \tag{12}$$

Using a similar variable change as in section 2.2, we obtain

$$S(f) = \sum_m e^{-\left(\left(mT_r\frac{2v}{c}\right)/\tau_0\right)^2} e^{-j2\pi mT_r\left(f-f_0\frac{2v}{c}\right)} e^{j\varphi} , \tag{13}$$

where $e^{j\varphi}$ is a non-important phase factor. The remainder of the right-hand term can be interpreted as the DTFT of the pulse $g\left(\frac{2v}{c}t\right) = e^{-\left(\left(\frac{2v}{c}t\right)/\tau_0\right)^2}$ (where $g(t)$ is the envelope of the original modulated pulse), shifted in frequency by $f_0\frac{2v}{c}$.

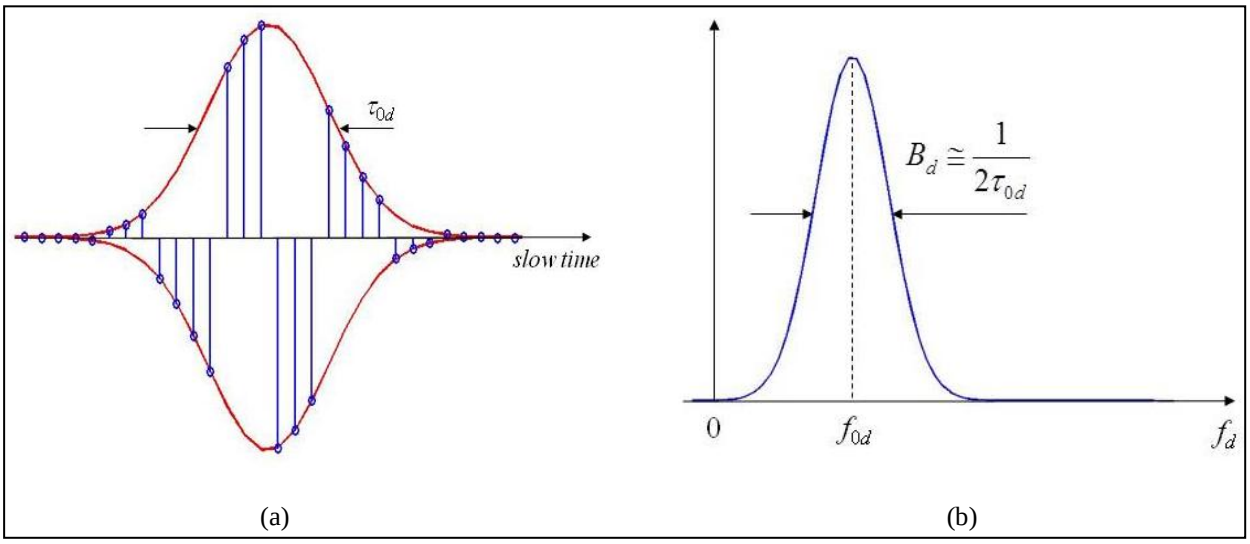

Figure 6. Representation of the sampled waveform in the slow-time and Doppler frequency domains, showing (a) pulse samples and envelope in the slow-time domain and (b) spectrum in the Doppler frequency domain. These plots correspond to a Gaussian-modulated pulse at transmission.

Consequently, the peak in the Doppler spectrum is located at f_{0d} given by

$$f_{0d} = f_0\frac{2v}{c}, \tag{14}$$

while the slow-time pulse width parameter τ_{0d} is

$$\tau_{0d} = \tau_0\frac{c}{2v}. \tag{15}$$

Notice that, formally, equations 9 and 14 are identical; however, as mentioned in section 2.2, the meaning of f_0 is different in the two cases.

2.4 Doppler Resolution and Performance Limits

The analysis presented in previous two sections did not make any assumption about the CPI, except for considering it as very large (compared to the duration of the sampled pulse in slow time). In reality, in conventional Doppler radar, the CPI is a critical parameter determining the Doppler resolution according to the equation (*2*)

$$\delta f = \frac{1}{\text{CPI}}. \tag{16}$$

However, the major difference between Doppler processing of UWB and narrowband pulses is that, in the former case, the CPI is longer than the slow-time pulse duration (a justification for this requirement is presented later in this section), whereas in the latter, the opposite is true. This difference is clearly illustrated graphically in figure 7, both in time and frequency domains.

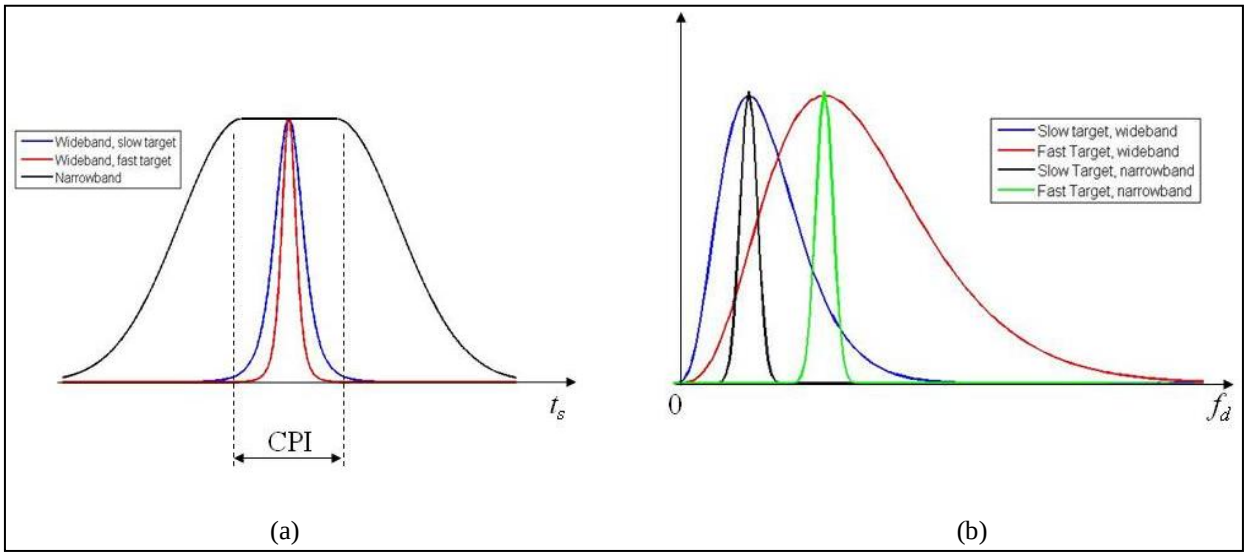

Figure 7. Comparison of Doppler processing using wideband and narrowband pulses, referenced to the length of a CPI, showing (a) slow-time domain representation of the pulse envelopes and (b) corresponding Doppler spectra.

Notice in figure 7a that the amplitude of the narrowband pulse envelope does not change much over the CPI. Instead, it is the phase variation over that interval that creates the peaks in the Doppler domain. As for the UWB pulses, the amplitude variation in slow time conveys significant information about the Doppler spectral content.

The fact that the non-zero data support processed in each STFT for the UWB case is shorter than the CPI means that the Doppler frequency resolution will be poorer than the limit given by equation 16. Moreover, for faster targets, the slow-time pulse duration is shorter than for slower targets, meaning that the Doppler resolution is further reduced as the target velocity increases. This is illustrated in figure 7b, which shows the broadening of the Doppler spectrum peak for the fast target. It is obvious that two targets with similar velocities would be more difficult to resolve in the Doppler domain when the peaks of their Doppler spectra are broad. Also notice that, for narrowband pulses, the Doppler resolution is independent of the target velocity.

We can express the Doppler frequency resolution for UWB pulses as the bandwidth of the slow-time pulse:

$$\delta f = B_d = \frac{2vB}{c}. \tag{17}$$

This expression shows that the Doppler resolution becomes poorer (δf larger) as either v or B increases. The velocity resolution is given by

$$\delta v = \delta f \frac{c}{2 f_0} = \frac{vB}{f_0}. \tag{18}$$

The widening of the Doppler spectrum peak (or loss of resolution) at higher velocities also implies that the peak's magnitude decreases proportionally when the target velocity increases. This effect may lead to a lower probability of detection of a fast target that needs to compete with either clutter or the sidelobes produced by another target placed nearby on the range-Doppler map.

Equation 18 suggests that UWB pulses, which by definition have large $\frac{B}{f_0}$ ratios, are in general ill-suited for target velocity estimation. Moreover, the velocity estimate resolution is dependent on the velocity itself. A possible solution to improve the velocity estimation resolution is to increase f_0 while keeping B constant. This amounts to modulating a high-frequency carrier (at the center frequency f_0) with a short baseband pulse. However, this case most likely constitutes a departure from the UWB impulse model described in section 2.1.

Figure 8 explains the reason why the CPI should normally exceed the slow-time pulse duration, by comparing the spectrum of a truncated pulse with that of its full-duration version for a 4th order Rayleigh waveform. If we use a Hanning window (*7*) in the STFT, the peak in the Doppler spectrum of the truncated pulse is slightly displaced with respect to the true peak. If we simply use a rectangular window for truncation, the Doppler spectrum exhibits large sidelobes, in addition to the peak shift. The effect of these sidelobes in the range-Doppler maps can be significant for range bins placed at the edges of the target trajectory over a CPI, hence they should be avoided.

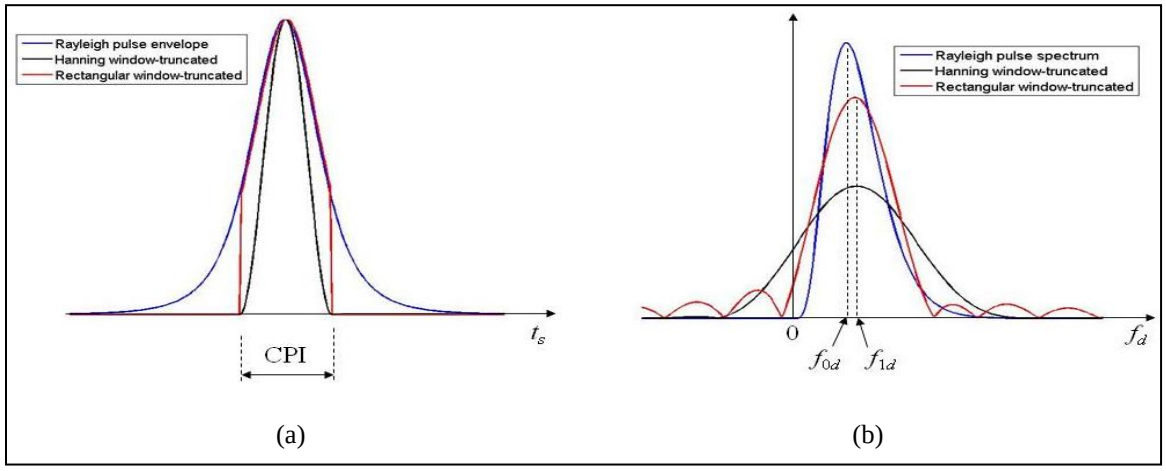

Figure 8. Illustration of the slow-time pulse truncation issue for baseband UWB pulses, showing (a) slow-time domain representation of the pulse envelope and (b) corresponding Doppler spectra.

The bias introduced in the Doppler spectrum peak by time-domain truncation is specific to pulses with asymmetric spectra (as in figure 1b) and does not affect waveforms with symmetric spectra (as in figure 2b). To demonstrate this, we repeat the previous analysis in figure 9, this time using a Gaussian-modulated pulse. We can see that, in the Doppler domain, the three peaks line up at the correct frequency. Moreover, the spectrum peak position is independent of the truncation window offset relative to the time-domain pulse envelope. The only negative effect is the widening of the peak, which is due to the reduced support of the STFT.

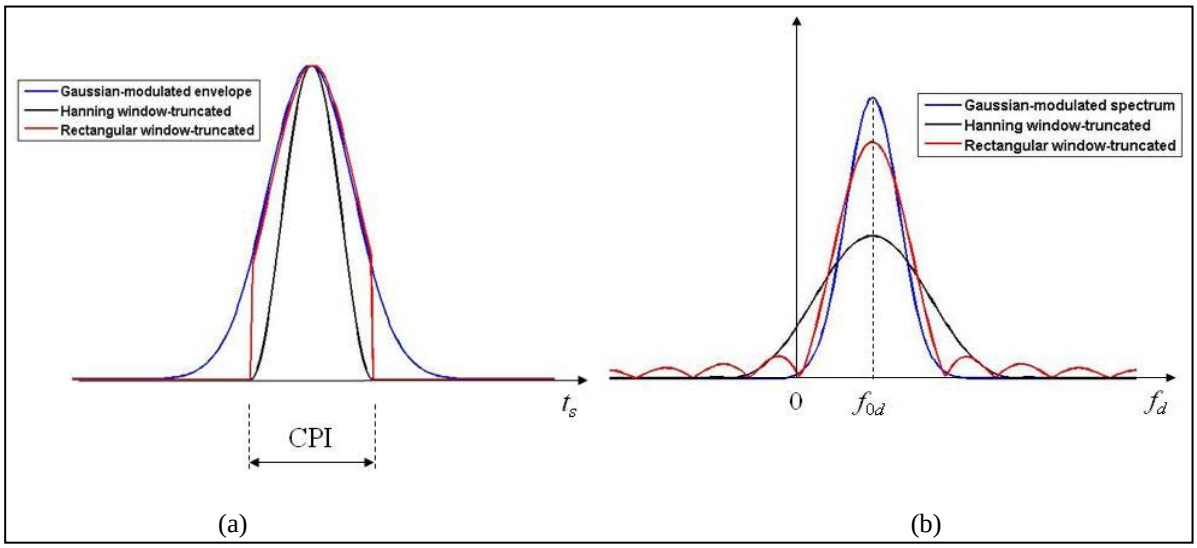

Figure 9. Illustration of the slow-time pulse truncation issue for modulated UWB pulses, showing (a) slow-time domain representation of the pulse envelope and (b) corresponding Doppler spectra.

We conclude that truncating the slow-time pulse (by choosing a CPI shorter than its duration) introduces a bias in the Doppler frequency estimate for baseband UWB pulses. To avoid this, each STFT should use a Hanning (or other smooth) window with an overall extent (between zero crossings) of about twice the longest slow-time pulse duration. This leads us to the idea of setting the CPI as a function of the minimum velocity of interest in the scene:

$$\mathrm{CPI} = \tau_{s\max} \cong \frac{c}{2|v_{\min}|B}. \tag{19}$$

Conversely, equation 19 allows us to determine the minimum velocity that can be reliably estimated with baseband UWB pulses given a certain value of the CPI. For modulated UWB pulses, there is no lower limit on the velocity that can be correctly estimated; however, there will be a loss of resolution for velocities below the value derived from equation 19.

Finally, the Doppler resolution analysis presented in this section allows us to establish a simple criterion to distinguish whether a pulse is narrowband or wideband with respect to Doppler processing. Specifically, if the target in motion covers less than a range bin during a CPI, then

we are in the narrowband regime; if the target covers a distance larger than a range bin during a CPI, then we are in the wideband regime.

3. Numerical Examples

3.1 Simulation Involving Baseband UWB Pulses

In this section, we present a simple numerical example obtained via simulation in MATLAB. It consists of two point targets moving in opposite directions, with radial velocities $v_1 = 0.4$ m/s and $v_2 = -0.6$ m/s (a positive velocity means the target moves towards the radar). The transmitted pulse is 4th order Rayleigh, with peak frequency $f_0 = 1$ GHz. The PRF is 40 Hz, while the total observation time is 2 s. The effective CPI is 0.6 s, and we use Hanning windows in the STFTs, with one slow-time sample shift from one CPI to the next for maximum overlap.

The original 2-D data array (as a function of range and time) is shown in figure 10, where we can see the two trajectories intersecting at one point in time. By performing the Doppler processing outlined in section 2.2 we obtain a collection of range-Doppler maps corresponding to successive slow-time intervals. Three of these maps, corresponding to time windows centered at 0, 1 and 2 s, respectively, are shown in figure 11.

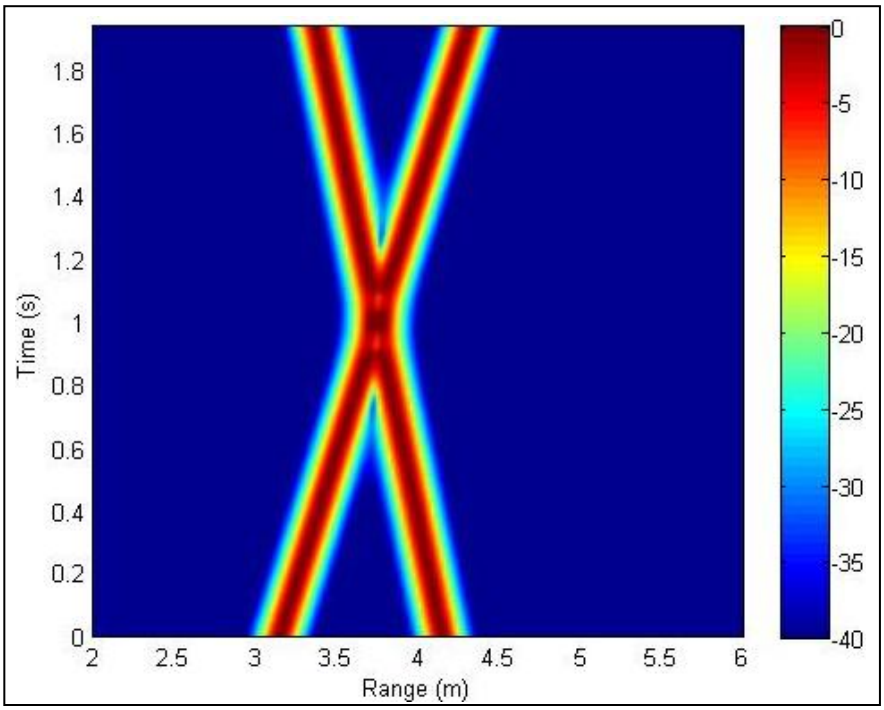

Figure 10. The 2-D received data array as a function of range and time for the simulation involving 4th order Rayleigh pulses at transmission.

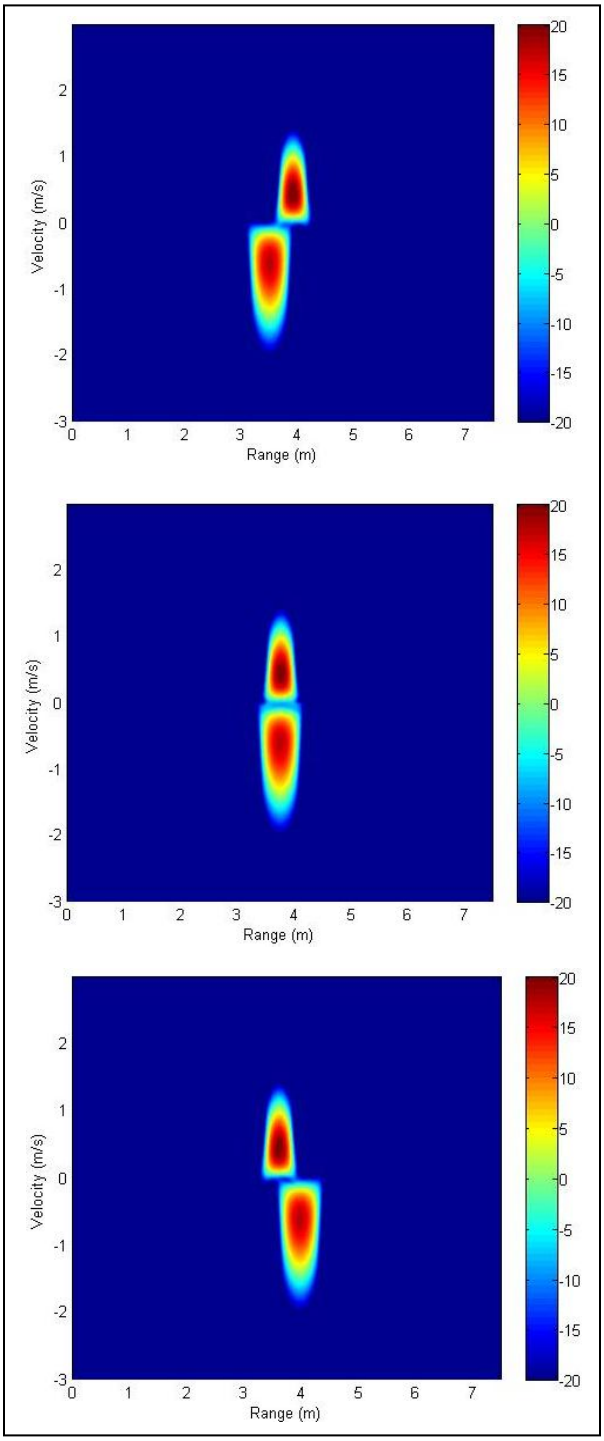

Figure 11. Range-Doppler maps obtained in the simulation involving 4th order Rayleigh pulses, corresponding to slow-time windows centered at 0, 1, and 2 s, respectively.

Notice that, in the range-Doppler maps in figure 11, the target with a larger velocity (in absolute value) displays a wider peak in the Doppler domain (poorer resolution). This effect was discussed in detail in section 2.4. Interestingly, the range-Doppler map peak corresponding to the

higher-velocity target also has a wider extent in range, showing a degradation of the resolution in this dimension. This can be easily explained by the fact that, in a UWB pulse regime, the target moves over more than one range bin during a CPI; therefore, the peak in the range-Doppler map is "smeared" over several original range bins. If the conventional range resolution is given by $\delta R = \frac{c\tau}{2}$, then, in a range-Doppler map created with UWB pulses, the new range resolution becomes

$$\delta_d R = v \times \mathrm{CPI} = \delta R \frac{\mathrm{CPI}}{\tau_s} > \delta R \,. \tag{20}$$

This equation shows that in a range-Doppler map obtained with UWB pulses the range resolution is poorer than in the original range profiles, and, moreover, this resolution depends on the target velocity (becomes worse for larger velocity). Even so, the range resolution achieved with UWB pulses after Doppler processing is better than the resolution achievable with narrowband pulses.

Figure 12 displays the JRTFR data cube mentioned in section 2.2. The two targets can be clearly separated in this picture, which was obtained by displaying only the points in the three-dimensional space whose magnitude exceeds a certain threshold (in our case, 15 dB). Notice that the resolution in both range and time dimensions is not as good as in the original 2-D data array (figure 10); however, the advantage of the JRTFR is that it adds a new dimension to the data (Doppler frequency), which can be useful in applications requiring target separation, discrimination or identification.

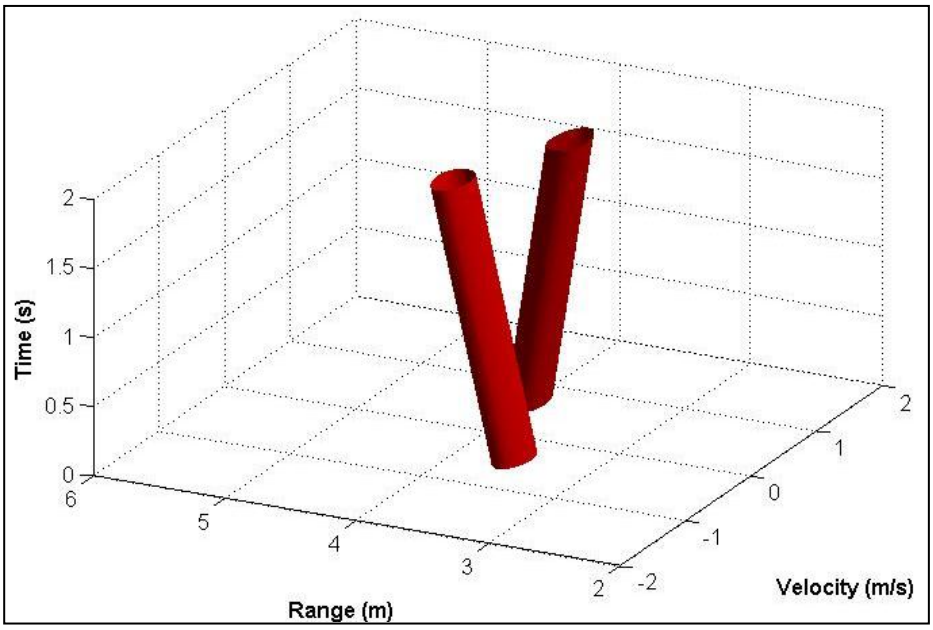

Figure 12. Representation of the JRTFR data cube obtained in the simulation involving 4th order Rayleigh pulses.

3.2 Simulation Involving Modulated UWB Pulses

We repeat the simulation in section 3.1, this time using a Gaussian modulated UWB pulse for transmission. All the parameters are identical to the previous case, except that the pulse has f_0 = 1.5 GHz and τ_0 = 500 ps. Since both the 2-D range-time data array and the JRTFR data cube look very similar with those in figures 10 and 12, we do not show these results in this section. Instead, we only concentrate on the range-Doppler maps, which display some slight differences with respect to figure 11.

Figure 13 plots the range-Doppler maps obtained for time windows centered at 0, 1, and 2 s. Similar to the simulation involving a Rayleigh (baseband) pulse, the resolution in poorer for larger target velocity, both in range and Doppler (the analysis goes the same as previously, with the exception that now, the Doppler peak width is given by the inverse of the τ_{0d} parameter). One noticeable difference is the fact that the targets have symmetric signatures on these range-Doppler maps, due to the symmetric nature of the pulse spectrum. Also, as explained in section 2.4, there are no minimum velocities involved in this type of Doppler analysis, since the estimates are unbiased for any velocity down to zero.

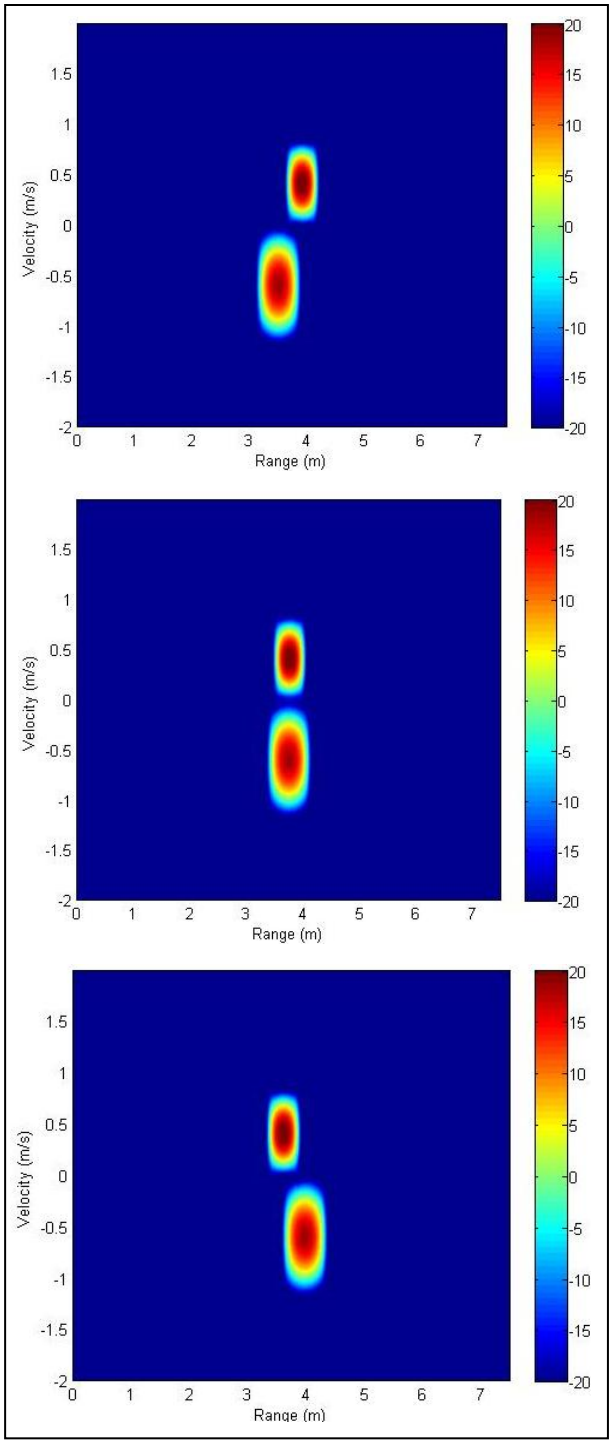

Figure 13. Range-Doppler maps obtained in the simulation involving Gaussian-modulated pulses, corresponding to slow-time windows centered at 0, 1, and 2 s, respectively.

4. Conclusions

In this note, we investigated the possibility of using UWB radar waveforms to estimate the velocity of a moving target. Specifically, we employed both baseband and modulated UWB impulses and a conventional range-Doppler map approach to simultaneously estimate the range and velocity of the target. As expected, these waveforms achieve excellent resolution in range, but poor resolution in the Doppler (velocity) domain. In section 2.4, we established theoretical expressions for the Doppler resolution, which degrades proportionally to the target velocity. We also found that, for baseband pulses, there is a minimum target velocity below which the Doppler domain estimation becomes unreliable (biased). Since the modulated UWB pulses are not affected by this issue, they are preferable to the baseband pulses for this type of analysis.

Although the conclusions of our analysis are mostly negative, it can be said that the technique described here can be applied to relatively slowly moving targets, in sparsely populated scenes (this would be combined with the requirement of short ranges, inherent to low-average-power UWB radar). The discrimination in range (and possibly in cross-range, for radars employing an antenna array), which can be performed with high accuracy, may be sufficient to distinguish between two targets, even though the Doppler resolution is poor.

A possible remedy to the poor Doppler resolution was indicated in section 2.4 and consists of increasing the "center frequency" f_0, without increasing the bandwidth. This amounts to using an UWB baseband pulse to modulate a high-frequency carrier (this is the approach used in reference 4)—in that case, the pulse may not be classified as UWB any longer, but still retains the high range resolution property. For example, if one uses a pulse centered at 10 GHz (X band) with the same bandwidth as the ones used in section 3 (which were "centered" around 1 GHz), the Doppler resolution increases tenfold.

Yet another possibility to measure the target velocity, which seems more natural for an UWB radar operating essentially in the time domain, is to compare the range profiles created at different moments in slow time (say, for instance, t_1 and t_2) and compute the average velocity as $\frac{R_2 - R_1}{t_2 - t_1}$. Note that this is a high resolution estimate, since R_2 and R_1 can be determined with high accuracy. If, additionally, one determines the cross-range position of the target as a function of time (for instance, via beamforming), this idea can be extended to compute the 2-D velocity vector. This is the approach used by Martone et al. (*8*) to track a person walking inside a room via STTW imaging radar.

5. References

1. Ressler, M.; Nguyen, L.; Koenig, F.; Wong, D.; Smith, G. The ARL Synchronous Impulse Reconstruction (SIRE) Forward-Looking Radar. *Proc. SPIE* **2007**, *6561*.
2. Skolnik, M. I. *Introduction to Radar Systems*; McGraw Hill: New York, 2001.
3. Smith, G. E.; Ahmad, F.; Amin, M. G. Micro-Doppler Processing for Ultra-wideband Radar Data. *Proc. SPIE* **2012**, *8361*.
4. Fogle, R.; Rigling, B. R. Micro-range/Micro-Doppler Decomposition of Human Radar Signatures. *IEEE Transactions on Aerospace and Electronic Systems* **October 2012**, *48*, 3058–3072.
5. Hubral P.; Tygel, M. Analysis of the Rayleigh Pulse. *Geophysics* **1989**, *54*, 654–658.
6. Haykin, S. *Communication Systems*; Wiley: New York, 1994.
7. Oppenheim, A. V.; Schafer, R. W. *Discrete-time Signal Processing*; Prentice Hall: Englewood Cliffs, NJ, 1989.
8. Martone, A.; Innocenti, R.; Ranney, K. *Moving Target Indication for Transparent Urban Structures*; ARL-TR-4809; U.S. Army Research Laboratory: Adelphi, MD, May 2009.

List of Symbols, Abbreviations, and Acronyms

2-D	two-dimensional
ARL	U.S. Army Research Laboratory
CPI	coherent processing interval
DC	direct current
DFT	discrete Fourier transform
DTFT	discrete-time Fourier transform
FOPEN	foliage penetration
GPR	ground penetrating radar
JRTFR	joint range-time-frequency representation
PRF	pulse repetition frequency
RF	radio frequency
SIRE	Synchronous Impulse Reconstruction
STFT	short-time Fourier transform
STTW	sensing through the wall
UWB	ultra-wideband

No. of Copies	Organization
1 (PDF only)	DEFENSE TECHNICAL INFORMATION CTR DTIC OCA
1 HC 9 PDFS	US ARMY RSRCH LAB ATTN IMAL HRA MAIL & RECORDS MGMT (1 HC) ATTN RDRL CIO LL TECHL LIB ATTN RDRL SER U M RESSLER A SULLIVAN C LE K RANNEY A MARTONE L NGUYEN D LIAO T DOGARU